Unconventional Giant "Magnetoresistance" in Bosonic Semiconducting Diamond Nanorings

Gufei Zhang,* Ramiz Zulkharnay, Xiaoxing Ke,* Meiyong Liao,* Liwang Liu, Yujie Guo, Yejun Li, Horst-Günter Rubahn, Victor V. Moshchalkov, and Paul W. May

The emergence of superconductivity in doped insulators such as cuprates and pnictides coincides with their doping-driven insulator–metal transitions. Above the critical doping threshold, a metallic state sets in at high temperatures, while superconductivity sets in at low temperatures. An unanswered question is whether the formation of Cooper pairs in a well-established metal will inevitably transform the host material into a superconductor, as manifested by a resistance drop. Here, this question is addressed by investigating the electrical transport in nanoscale rings (full loops) and half loops manufactured from heavily boron-doped diamond. It is shown that in contrast to the diamond half-loops (DHLs) exhibiting a metal–superconductor transition, the diamond nanorings (DNRs) demonstrate a sharp resistance increase up to 430% and a giant negative "magnetoresistance" below the superconducting transition temperature of the starting material. The finding of the unconventional giant negative "magnetoresistance", as distinct from existing categories of magnetoresistance, that is, the conventional giant magnetoresistance in magnetic multilayers, the colossal magnetoresistance in perovskites, and the geometric magnetoresistance in semiconductor–metal hybrids, reveals the transformation of the DNRs from metals to bosonic semiconductors upon the formation of Cooper pairs. DNRs like these could be used to manipulate Cooper pairs in superconducting quantum devices.

1. Introduction

Materials can be roughly categorized by their electronic properties into insulators, semiconductors, conductors, and superconductors. As the temperature decreases, insulators, having a wide band gap, demonstrate a pronounced increase in their electrical resistance that diverges at zero temperature. Semiconductors have a narrower band gap, and their resistance also increases with a decrease in temperature, which is generally less pronounced than that of insulators. Metals without a band gap are mostly good electrical conductors and generally show a positive temperature coefficient of resistance above a finite temperature, below which their resistance becomes temperature-invariant (known as the residual resistance). Superconductors are located at the opposite extreme to insulators in conductivity. At low temperatures, a superconducting gap opens at the Fermi energy, where the free electrons are bound into Cooper pairs, and the condensation

G. Zhang, H.-G. Rubahn
Danish Institute for Advanced Study and Mads Clausen Institute
University of Southern Denmark
Alsion 2, Sonderborg DK-6400, Denmark
E-mail: gufei@mci.sdu.dk

R. Zulkharnay, P. W. May
School of Chemistry
University of Bristol
Bristol BS8 1TS, UK

X. Ke
Faculty of Materials and Manufacturing
Beijing University of Technology
Beijing 100124, China
E-mail: kexiaoxing@bjut.edu.cn

M. Liao
Research Center for Functional Materials
National Institute for Materials Science (NIMS)
Namiki 1-1, Tsukuba, Ibaraki 305-0044, Japan
E-mail: meiyong.liao@nims.go.jp

L. Liu
Laboratory for Soft Matter and Biophysics
Department of Physics and Astronomy
KU Leuven, Heverlee B-3001, Belgium

Y. Guo
Photonics Research Group, Department of Information Technology
Ghent University-IMEC
Ghent 9052, Belgium

Y. Li
Hunan Key Laboratory of Nanophotonics and Devices, School of Physics
& Electronics and School of Materials Science & Engineering
Central South University
Changsha 410083, China

V. V. Moshchalkov
Department of Physics and Astronomy
KU Leuven, Heverlee B-3001, Belgium

2211129 (1 of 10)

of the Cooper pairs gives rise to a zero-resistance macroscopic quantum state, that is, superconductivity.

Given the discoveries of superconductivity in various materials which are either intrinsically metallic or doped insulators located on the metallic side of their insulator–metal transitions (e.g., cuprates,[1,2] pnictides,[2–4] transition-metal oxides,[5–7] and diamond[8,9]), an established metallic state appears to be a prerequisite for the emergence of superconductivity. These metallic systems feature a variety of resistive superconducting transitions, for example, significantly broadened transitions in highly disordered systems, and two-step resistance drops in the case of short- and long-range phase coherences or in the presence of impurity phases.[1,5,9–12] Despite different features specific to the host system, such conventional superconducting transitions manifest themselves as a monotonic decrease in resistance below the critical temperature, T_c.

The transformation from a metal to a superconductor, however, does not always proceed as a monotonic resistance decrease. Occasional observations of a narrow resistance peak preceding the onset of the superconducting state have been reported for some materials and low-dimensional microstructures. For example, resistance peaks with an amplitude of 10–340% were observed in 1D and 2D mesoscopic structures made of Al or AuIn alloy.[13–17] Similar effects with a peak amplitude in the range of 16–700% were found in quasi-2D cuprates such as NdCeCuO,[18,19] PrCeCuO,[18] LaSrCuO,[19,20] and BiSrCaCuO.[21,22] These resistance anomalies were mostly attributed to the reduced dimensionality of the host system, which, however, cannot be theoretically reconciled with similar observations in 3D materials, for example, resistance peaks with an amplitude of 3% in CuZr alloys,[23] 4% in an Nb foil,[24] 15% in a diamond film ,[25] and in particular the giant narrow peaks (up to 1600%) observed in thick polycrystalline diamond layers.[26]

Here, we present electrical transport measurements on 3D nanoscale rings and half-loops fabricated from heavily boron-doped diamond thin films (DTFs)that are located deeply on the metallic side of the insulator–metal transition. We observe that below the T_c of the starting materials, the diamond half-loops (DHLs)show a resistance drop to zero, whereas the diamond nanorings (DNRs) demonstrate a sharp increase in resistance (up to 430%). Furthermore, when approaching zero temperature, the DNRs exhibit a high-resistance state well above their residual resistance, rather than transforming into superconductors. Upon the suppression of the high-resistance state in the DNRs by using high magnetic fields, giant negative "magnetoresistance" emerges along with the restoration of the metallic normal state. Our results suggest that when approaching zero temperature, other than the well-studied resistive superconducting transitions (decrease of resistance) and quantum metallic states (invariance of resistance),[27] there is a third route (increase of resistance) with which an established metal can proceed upon the formation of Cooper pairs.

2. Results and Discussion

2.1. Diamond Nanorings Fabricated from Superconducting Diamond Thin Films

Our samples are fabricated from 850nm-thick polycrystalline DTFs with a boron concentration of about 3.3×10^{21} cm^{-3}.

The DTFs, deposited on SiO_2/Si substrates using chemical vapor deposition (CVD) (see Experimental Section),[28] consist of columnar diamond crystallites separated by grain boundaries containing a few atomic layers of amorphous carbon and boron.[29] **Figure 1**a shows the Raman spectrum of the DTFs. Due to the Fano effect, the high boron concentration causes a distortion in the shape of the first-order diamond phonon line and a shift in its position from 1332 to 1295 cm^{-1} (red arrow) such that it appears as a shoulder on the large boron-related feature around 1200 cm^{-1}.[30]

Cost-effective polycrystalline diamond films grown on non-diamond substrates generally have a large surface roughness comparable to the film thickness due to the growth mode of this material.[28,29] Through atomic force microscopy (AFM) imaging, the surface roughness of our DTFs is demonstrated to be around 400 nm (inset to Figure 1a). From statistics of the grain size distribution, the mean grain size of the DTFs is deduced to be about 600 nm (Figure 1b) (see Experimental Section).

In contrast to disorder-free superconductors featuring a sharp resistance drop at T_c, the DTFs show a rather broad resistive superconducting transition in the temperature dependence of resistance, $R(T)$, which onsets at 4.4 K and offsets at 3.2 K (Figure 1c). The extraordinarily broad superconducting transition results from the weak coupling between the superconducting diamond grains in the presence of high-resistance grain boundaries. When increasing the temperature, the gap in the magnetic-field dependence of resistance, $R(H)$, is smeared out, and the metallic nature of the DTFs is restored, due to the decoupling between the diamond grains and the breaking of Cooper pairs (Figure 1d).

It is quite challenging to manufacture polycrystalline diamond films with a large surface roughness such as our DTFs into DNRs by using lithography alone. To overcome the challenge, we first patterned the DTFs into microcrosses consisting of 1.5μm-wide diamond wires by using lithography combined with oxygen plasma etching, and then etched these into DNRs with a focused Ga ion beam (**Figure 2**a–c) (see Experimental Section). The as-prepared DNRs consist of polycrystalline diamond tracks (henceforth called "wires") with a width of 220 ± 50 nm. Taking into account the disorder introduced in the walls during Ga ion milling, the effective width of the constituent diamond wires is estimated to be 200 ± 50 nm based on SRIM simulation.[31] The DNRs consist of a hollow square of diamond wire, with inside dimensions of about 280 × 280 nm and outside dimensions of ≈720 × 720 nm, with four wires attached around the outside as electrical leads for four-probe measurements. The two wires on the center of two of the opposite sides are used to send current so that charge carriers flowing through a DNR can take two alternative routes, clockwise or counterclockwise. Here, we present the data of two DNRs (labeled DNR1 and DNR2, for confirmation of repeatability), deposited and patterned under identical conditions, showing the characteristic electrical transport behavior of our samples. We note that the DNRs are in the 3D regime, due to the remarkable difference between their dimensions and the minute coherence length of superconducting diamond (<15 nm).[32]
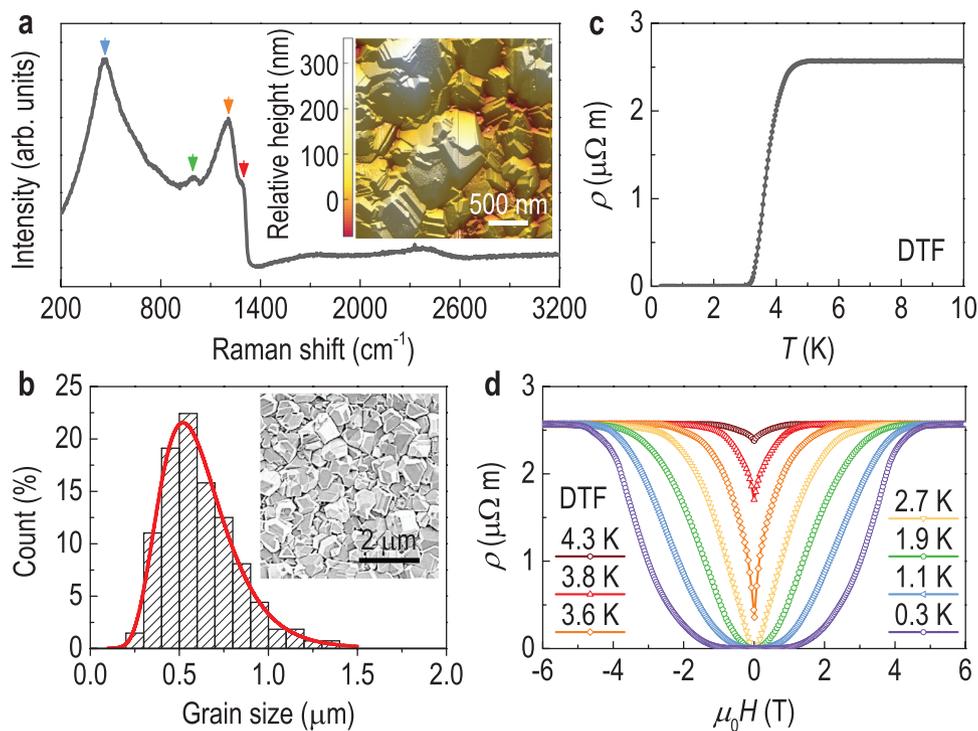
Figure 1. Characterization of the heavilyboron-doped polycrystalline DTF used as the starting material. a) Laser Raman spectrum measured with 514 nm excitation. Blue arrow: Vibrations of boron dimers and/or clusters. Green arrow: The minimum of the phonon density of diamond and a characteristic feature of boron-doped diamond. Orange arrow: Defects in the diamond lattice caused by heavy boron doping. Red arrow: The first-order diamond phonon line. Inset: AFM image illustrating the granular nature and surface topology of the DTF. b) Grain size statistics (bar chart) obtained through analysis of a SEM image (inset). The grain size follows a lognormal distribution as shown by the fitting (red curve). c) Resistivity versus temperature, $\rho(T)$, showing the temperature-induced metal–superconductor transition measured at zero magnetic field. d) Resistivity versus magnetic field, $\rho(T)$, showing the magnetic-field-driven superconductor-metal transition measured at different temperatures.

2.2. Anomalous Resistance Increase and Unconventional Giant "Magnetoresistance" in Diamond Nanorings

The DNRs show an $R(T)$ distinctly different from that of the starting material (Figure 2d). Below the T_c of the DTFs, the $R(T)$ of the DNRs first overshoots the residual resistance by 260–430%, which turns into a decrease at lower temperatures and then regains its increasing trend below about 1 K. These unconventional $R(T)$ behaviors distinguish themselves from previously reported data in the following three aspects: 1) despite its similarity to the metal–insulator transition in materials such as VO$_2$,[33] the sharp $R(T)$ increase implies its correlation with resistive superconducting transition in the starting material by onsetting at about T_c, and thus cannot be viewed as a fermionic transition; 2) in contrast to the low-temperature bosonic insulating states in highly disordered superconductors with a weakly insulating normal state,[34] the sharp $R(T)$ increase in the DNRs evolves from an established metallic normal state; 3) when approaching zero temperature, $R(T)$ remains well above the residual resistance value and regains its increasing trend at low temperatures, rather than evolving into a superconducting transition as in the previously reported narrow resistance peaks.[13–26]

To elucidate the bosonic nature of the $R(T)$ anomaly in the DNRs, we measure the $R(H)$ at different temperatures. As shown in Figure 1d and **Figure 3**, respectively, the $R(H)$

of the DTFs acts as an increasing function of the applied magnetic field below T_c, whereas the behavior of the $R(H)$ of the DNRs is nearly opposite to that of the DTFs, and bears great resemblance to the conventional giant negative magnetoresistance in alternating ferromagnetic and non-magnetic layers,[35] that is, a giant resistance peak centered at zero magnetic field with two shoulders flattening out at high magnetic fields. Note that despite the nearly identical dimensions of DNR1 and DNR2, their structural imperfections induced in the ion milling process and the grain boundaries in their constituent diamond nanowires are different, which may be the cause of the difference in amplitude of their $R(T)$ and $R(H)$ anomalies.

The bosonic nature of the giant negative "magnetoresistance" is indicated by the following key features of the data: 1) At temperatures well below T_c, a minute zero-field gap is superimposed on the giant $R(H)$ peak (Figure 3). This gap, which highly likely results from short-range phase coherence (coupling between some of the grains in the constituent diamond nanowires), closes at higher temperatures. Along with the closing of the gap (breaking of the short-range phase coherence), the giant $R(H)$ peak regains its increasing trend at zero magnetic field. 2) As the temperature increases, the giant $R(H)$ peak is significantly suppressed. Upon the disappearance of the $R(H)$ peak at T_c, the normal metallic state is restored in the DNRs.
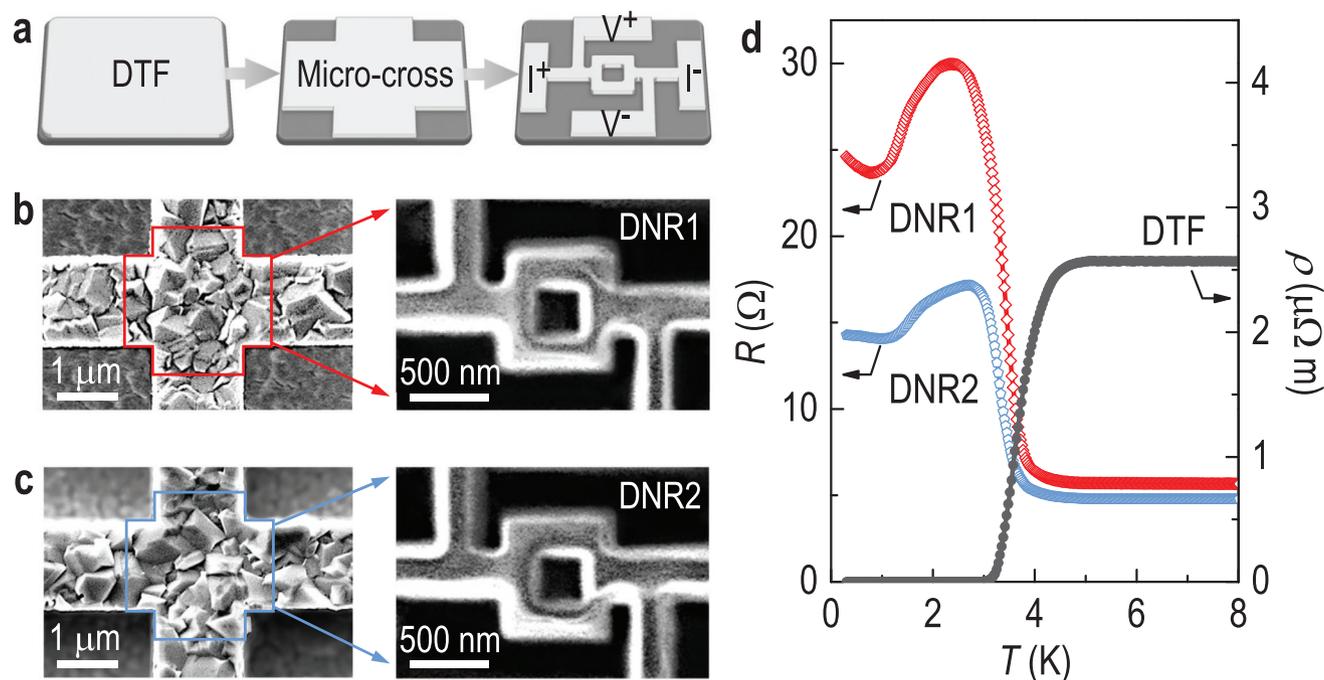
Figure 2. Anomalous temperature-dependent resistive transitions in DNRs fabricated from the superconducting polycrystalline DTFs. a) Schematic illustration of the fabrication process and the electrical configuration for transport measurements. b,c) SEM images of two DNRs, DNR1 and DNR2, which are fabricated from two microcrosses, respectively, through focused ion beam milling. Due to redeposition in the ion milling process, the constituent nanowires of the DNRs are enshrouded by a thin layer of high-resistance amorphous carbon, making the ultrathin grain boundaries invisible (see Experimental Section). d) Plot of resistance versus temperature, $R(T)$, for the diamond nanorings, revealing an anomalous resistance increase below the T_c of the starting material.

2.3. Resistive Superconducting Transition and Conventional Magneto-Transport in Diamond Half-Loops

To clarify whether the anomalous $R(T)$ increase and the unconventional giant negative "magnetoresistance" in the DNRs are caused by the patterning of the DTFs into diamond nanowires or, alternatively, by the full-loop structure of the DNRs, we manufactured the same starting material into DHLs which are nearly identical to the DNRs except that only half the square is present, thus only one current pathway is possible (**Figure 4**a).

In striking contrast to the DNRs, despite being composed of nearly identical diamond nanowires, the DHLs exhibit a rather conventional resistive superconducting transition as in the DTFs except that the transition is significantly broadened with its offset critical temperature shifted down to about 0.7 K (Figure 4b). A polycrystalline DTF can be treated as a 2D network of weak links, where the formation of a quantum condensate of charged bosons proceeds through intragrain Cooper pairing followed by intergrain coupling. When patterning a 2D network into a 1D chain of weak links, such as the constituent diamond nanowires of the DHLs and DNRs, the intergrain coupling is constrained to take place along the nanowires due to the truncation of other percolation paths. The zero-resistance state sets in only under the circumstance that long-range phase coherence is established across the device via intergrain coupling. Apart from the reduction of percolation paths, disorder induced by Ga ion milling can also add to the cause of the extraordinarily broad resistive superconducting transition in the DHLs by perturbing both Cooper pairing and intergrain coupling.

Consistent with their resistive superconducting transitions in $R(T)$, the DHLs show a gap rather than a peak in the $R(H)$ below T_c (Figure 4c–f). At low temperatures, the DHLs exhibit a two-step-like transition in $R(H)$ where the low-field part of the transition features a larger magnetic field coefficient of resistance than that of the high-field part. This is because the superconductivity in the vicinity of the walls of the constituent diamond nanowires is substantially degraded during the Ga ion milling process and can be easily destroyed by low magnetic fields, whereas the central part of the diamond nanowires remains intact, thus providing a more robust percolation path that persists in higher magnetic fields.

2.4. Diamond Nanorings Compared with Diamond Half-Loops for their Current Dependence of Voltage and Phase Boundaries

The nearly opposite behaviors of the DNRs and DHLs in electrical transport are further evidenced by our measurements of the current dependence of voltage, $V(I)$. As shown in **Figure 5**, below T_c and in low magnetic fields, the $V(I)$ curves of DNR1 and DHL1 demonstrate upward and downward deviations, respectively, from their linear $V(I)$ dependences of the metallic normal state. The increase in temperature (Figure 5a,b) and applied magnetic fields (Figure 5c,d) lead to the reduction of the deviations, due to the extinction of Cooper pairs.

Figure 6 shows the phase boundaries extracted from the $R(H)$ measurements on the DNRs, the DHLs, and the DTF. By setting the criterion at 105% of the residual resistance for the determination of the onset critical magnetic field of the $R(H)$
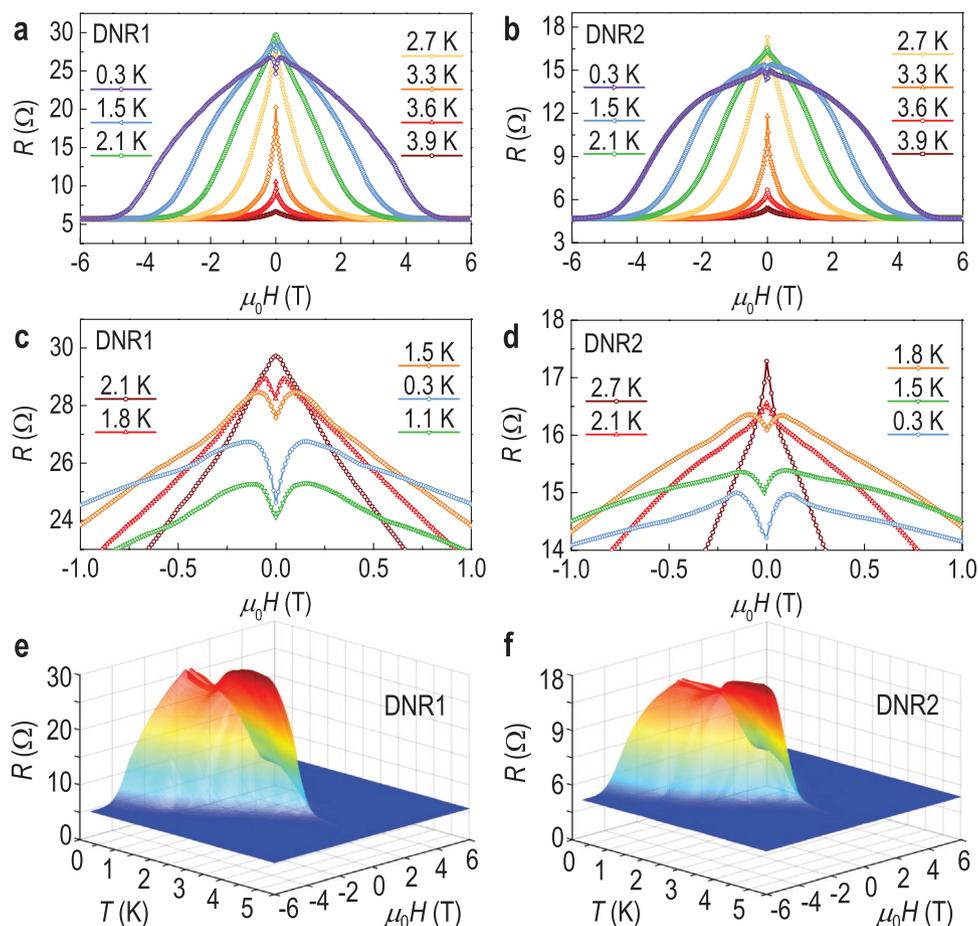
**ADVANCED
SCIENCE NEWS**

www.advancedsciencenews.com

**ADVANCED
MATERIALS**

www.advmat.de

Figure 3. Unconventional giant negative "magnetoresistance" in DNRs. a,b) Temperature-induced evolution of the unconventional giant "magnetoresistance" in DNR1 and DNR2. The "magnetoresistance" fades away when the temperature approaches T_c. c,d) At low temperatures, a minute gap is superimposed on the giant "magnetoresistance" peak. e,f) 3D view of the giant "magnetoresistance" peak in the $R(T,H)$ space.

peak (Figure 3), we build up the H–T phase boundaries of the DNRs. As shown in Figure 6, the phase boundaries of the DNRs almost coincide with the H_{c2}–T phase boundaries of the DTF and DHLs [the upper critical magnetic field, H_{c2}, is determined by setting the criterion at 95% of the residual resistance (Figures 1d and 4c–f)]. The extrapolation of these phase boundaries down to zero temperature through quadratic fitting yields nearly the same Ginzburg-Landau coherence length, ξ_{GL}, for our samples, that is, 8.6 nm in the DTF, 8.2 nm in DHL1, 8.4 nm in DHL2, 8.0 nm in DNR1, and 7.9 nm in DNR2, provided that the emergence of the $R(H)$ peaks in the DNRs is, indeed, driven by Cooper pairs. Our data suggest that in stark contrast to the conventional magnetoresistance originating from spin-dependent scattering of single electrons in layered systems, the giant negative "magnetoresistance" in the DNRs results from unconventional behavior of Cooper pairs.

2.5. Modeling of the Bosonic Semiconducting Transition in Diamond Nanorings

Because the nearly opposite behaviors of the DNRs and DHLs in $R(H)$ and $V(I)$ are directly linked to their differences in $R(T)$,

the elucidation of their resistive transitions below T_c will provide critical insight into the anomalous electrical transport properties of the DNRs. As shown in Figures 2d and 4b, below T_c, the DNRs and the DHLs embark on two opposite paths upon the formation of Cooper pairs, that is, a resistance increase with bosonic nature in the DNRs versus a resistive superconducting transition in the DHLs. The bosonic resistance increase in the DNRs demonstrates a temperature coefficient smaller than that of the previously reported bosonic insulating states,[26,34] and thus we term it a bosonic semiconducting transition. The transformation of the DNRs from metals to bosonic semiconductors is most likely driven by the trapping of Cooper pairs, otherwise, the DNRs would have shown a similar resistive superconducting transition as in the DHLs. Below T_c, Cooper pairs are formed at the expense of electrons at the Fermi energy. In the case that the Cooper pairs are trapped in the DNRs and do not flow through the devices, the depletion of free electrons will give rise to a metal–bosonic semiconductor transition. Upon the application of magnetic fields, the Cooper pairs trapped within the DNRs are broken, and single electrons are released at the Fermi energy, leading to the decrease of resistance and thus the emergence of giant negative "magnetoresistance" (Figure 3). At high magnetic fields, the extinction
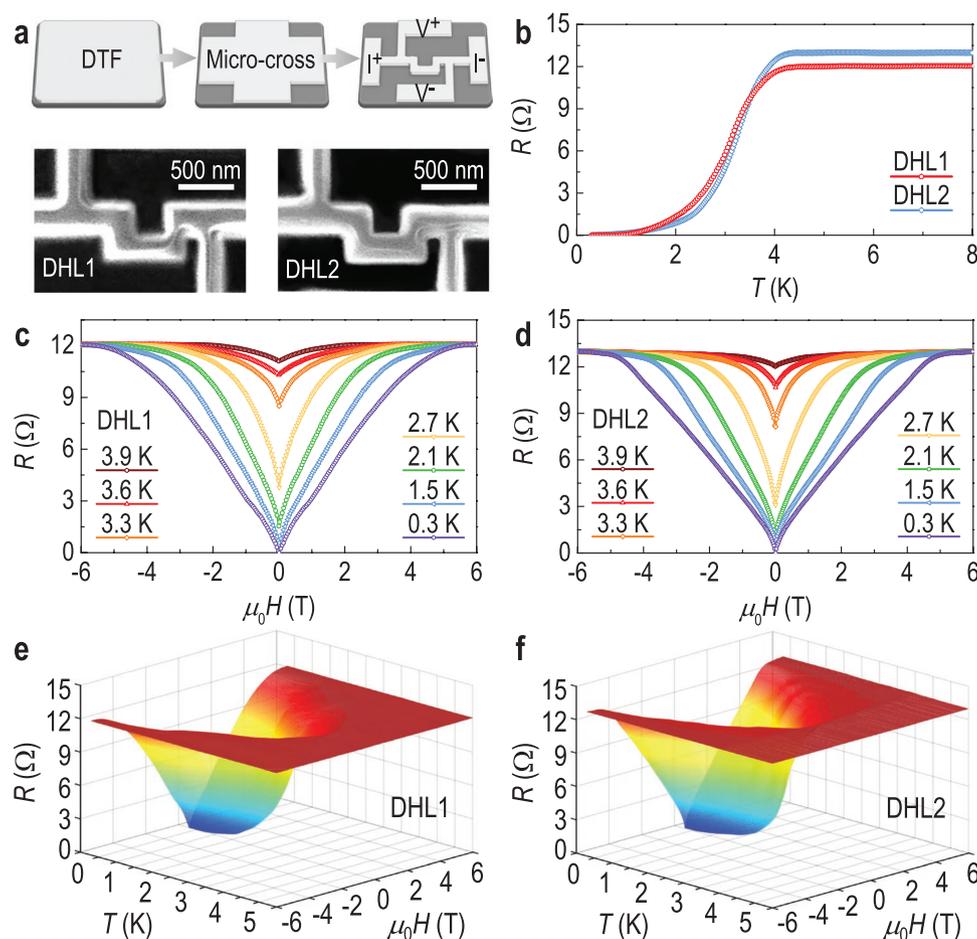
Figure 4. Conventional resistive superconducting transition in nanoscale DHLs. a) Schematic illustration of the fabrication of DHLs and SEM images of the DHLs. The DHLs are nearly identical to the DNRs except that only one pathway is provided for Cooper pairs to travel. b) Temperature-driven resistive superconducting transition in the DHLs. c,d) Temperature-induced evolution of the resistive superconducting gap in $R(H)$. e,f) 3D view of the resistive superconducting gap in the $R(T,H)$ space.

of trapped Cooper pairs leads to the complete release of single electrons and thus the restoration of the metallic normal state. This scenario also applies to the $V(I)$ dependences of DNRs. At low temperatures or in low magnetic fields, the trapping of Cooper pairs in the DNRs results in an upward deviation of the $V(I)$ curve from the linear dependence of the metallic normal state (Figure 5). When the trapped Cooper pairs are broken by increased temperature or magnetic fields, the deviation diminishes due to the release of single electrons.

Hypothetically, measurements of the Hall effect of the DNRs would provide direct evidence for the depletion of single electrons upon the formation of trapped Cooper pairs. Unfortunately, neither a Hall bar structure nor the van der Pauw method can be used to measure the Hall effect of the DNRs. A Hall bar structure can be only used to measure the Hall effect of the constituent nanowires of the DNRs rather than probing the Hall voltage across a DNR. The van der Pauw method cannot be applied to samples with non-uniform thickness or holes.

Upon a superconducting transition, the dominance in electrical transport is transferred from single electrons to Cooper pairs. Theoretically, such a transfer can be realized by making

use of the switch-like function of a two-channel parallel-circuit model,

$$R_t = \frac{R_f R_b}{(R_f + R_b)} \tag{1}$$

where R_t, R_f, and R_b are, respectively, the total resistance of the circuit, the resistance of the fermionic channel, and the resistance of the bosonic channel.[26] At T_c, a superconducting gap, Δ, opens at the Fermi energy, E_F, and the free electrons around E_F are bound into Cooper pairs.

Regardless of the microscopic mechanism, as long as the Cooper pairs are trapped within the DNRs, the depletion of free electrons will exert its influence on the resistance of the fermionic channel, R_f, as shown by the integral in

$$R_f(T) = R_r \left[-2 \int_{\Delta(T)}^{\infty} g(E) f'(E) dE \right]^{-1} \tag{2}$$

where R_r is the residual resistance of the metallic state, $g(E) = E[E^2 - \Delta(T)^2]^{-0.5}$ is the density of states in the

ADVANCED
SCIENCE NEWS
www.advancedsciencenews.com
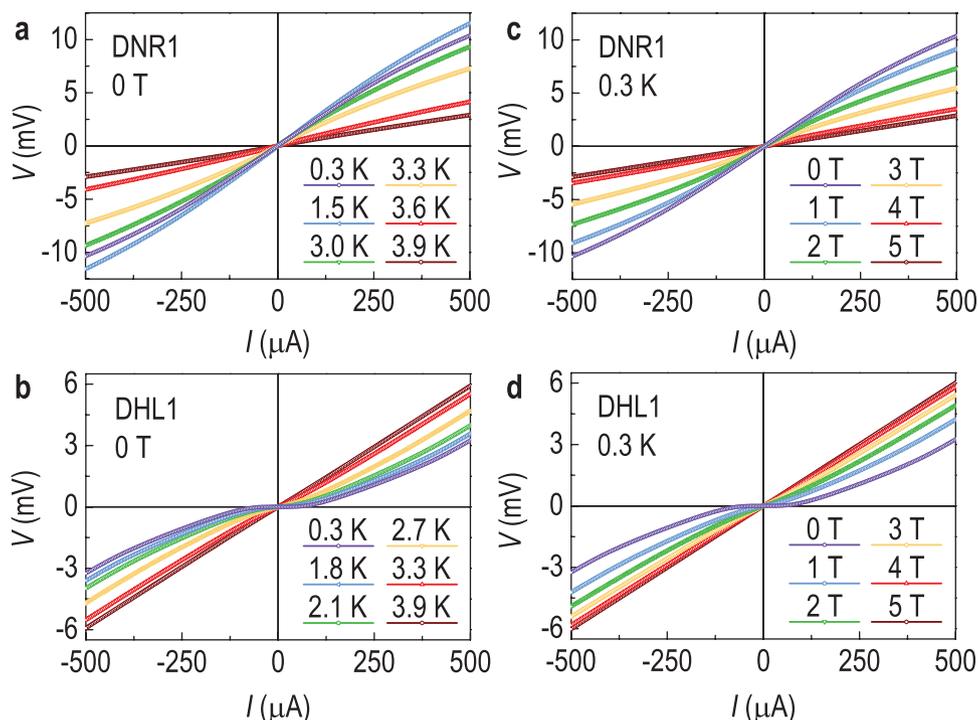
ADVANCED
MATERIALS
www.advmat.de

Figure 5. DNRs compared with DHLs for their current dependence of voltage, $V(I)$. a,b) $V(I)$ dependences measured at different temperatures in zero magnetic field. c,d) $V(I)$ dependences measured in different magnetic fields at 0.3 K. At low temperatures and in low magnetic fields, the $V(I)$ curves of DNR1 and DHL1 deviate from the linear $V(I)$ dependences of their metallic normal state in opposite directions, that is, an upward deviation in DNR1 versus a downward deviation in DHL1.

Bardeen–Cooper–Schrieffer (BCS) theory, and $f'(E)$ is the derivative of the Fermi–Dirac distribution. The depletion of single electrons at E_F, due to the formation of trapped Cooper pairs below T_c, is illustrated schematically in **Figure 7**a. Close to T_c,

$\Delta(T)$ can be approximated by $\Delta^*(T) = \Delta^*(0 \text{ K})[1 - T/T_c]^{0.5}$ with $\Delta^*(0 \text{ K}) = 1.74\Delta(0 \text{ K})$.[26,36]

The trend of increasing resistance of the DNRs is interrupted by a finite resistance drop below $\approx$2.5 K (Figure 7b), indicating the competing interplay between the fermionic and bosonic channels. The resistance drop is most probably caused by short-range phase coherence (coupling between some of the superconducting grains) in the DNRs. Empirically, the resistance of the bosonic channel can be written as

$$R_b(T) = R_0 + R_s\left(\frac{T}{T^*} - 1\right)^\eta \qquad (3)$$

where R_0 is the offset resistance, the prefactor, R_s, and the exponent, η, describe the sharpness of the resistive superconducting transition, and T^* is the offset temperature of the transition. When Cooper pairs condense into a macroscopic zero-resistance state with long-range phase coherence at T^*, $R_0 = 0$.

As shown in Figure 7b, the two-channel model captures well the key features of the transport properties of the DNRs. By setting = 3.9 K, $T^* = 0.8$ K, $R_r = 5.8$ Ω, and $R_0 = 23.7$ Ω as fixed parameters, we obtain $\Delta(0 \text{ K}) = 1.3$ meV, $R_s = 2.3$ Ω, and $\eta = 1.9$ for DNR1 through fitting. For DNR2, $\Delta(0 \text{ K}) = 1.4$ meV, $R_s = 1.2$ Ω, and $\eta = 1.8$ are obtained from the fitting by using $T_c = 3.8$ K, $T^* = 0.9$ K, $R_r = 4.9$ Ω, and $R_0 = 14.1$ Ω. These fittings yield $2\Delta(0 \text{ K})/k_B T_c$ ratios of 7.9 for DNR1 and 8.4 for DNR2, respectively, in contrast to the universal value of 3.53 predicted by the BCS theory. We note that extraordinarily large $2\Delta(0 \text{ K})/k_B T_c$ ratios have been experimentally demonstrated
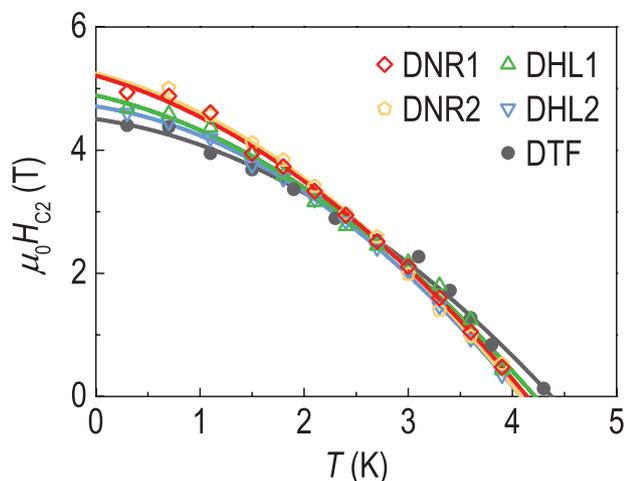

Figure 6. Phase boundaries of DNRs, DHLs, and the starting material. The temperature dependences of the onset critical magnetic fields of the giant "magnetoresistance" peaks in DNR1 and DNR2 (Figure 3) nearly coincide with the H_{c2}–T phase boundaries of DHL1, DHL2, and the starting material, indicating the bosonic nature of the unconventional giant "magnetoresistance" in the DNRs. The phase boundaries are extrapolated down to zero temperature through quadratic fits (curves).

**ADVANCED
SCIENCE NEWS**

www.advancedsciencenews.com
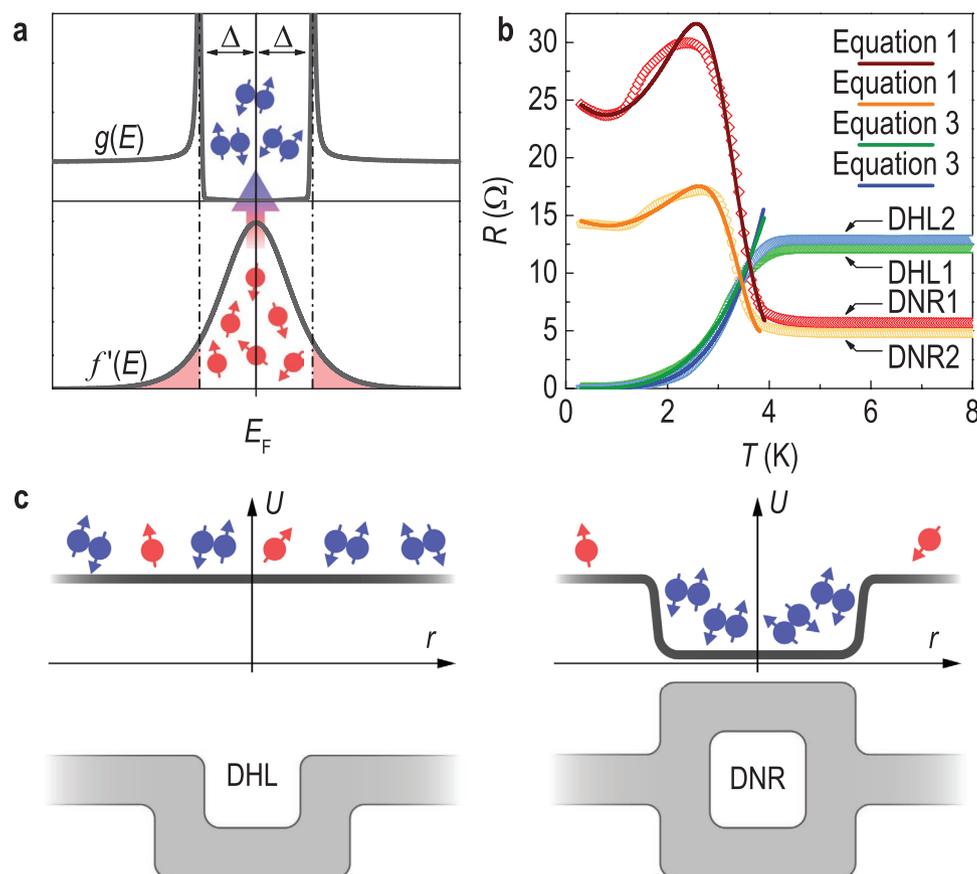
**ADVANCED
MATERIALS**

www.advmat.de

Figure 7. Metal–bosonic semiconductor transition driven by the trapping of Cooper pairs in DNRs. a) Schematic interpretation of the depletion of single electrons (red) at E_F as a result of the formation of Cooper pairs (blue). As denoted by the arrow, below T_c the single electrons at E_F are bound into Cooper pairs, giving rise to a superconducting gap at E_F. If the Cooper pairs are trapped within a DNR, the bosonic channel of the device will be closed, and only the fermionic channel can contribute to the electrical transport through the device by making use of the remaining single electrons in the vicinity of E_F [the shoulders of $f'(E)$ highlighted in light red]. b) Modeling of the resistive transitions in DNRs and DHLs. The bosonic semiconducting transition in DNRs is fitted by a two-channel parallel circuit model [Equation (1)]. The resistive superconducting transition in DHLs is fitted by an empirical power law [Equation (3)]. c) Schematic illustration of the flow of single electrons and Cooper pairs through a DHL and a DNR. Our data suggest that although disorder, such as the grain boundaries and the surface damage caused by ion milling, perturbs the spatial dependence of the potential, $U(r)$, Cooper pairs can still flow through a DHL, whereas a DNR effectively acts as a quantum well which traps Cooper pairs. The trapping of Cooper pairs leads to the emergence of the metal–bosonic semiconductor transition and thus the unconventional giant "magnetoresistance" below T_c.

for various systems, for example, 6.5–11.5 in InO,[37] 12.3 in BiSrCaCuO,[38] 16.6 in BiOS,[39] and 28 in BiSrCuO.[40]

The resistive superconducting transition in the DHLs is described well by Equation (3) alone (Figure 7b). Using the experimental value of $T^* = 0.7$ K, $R_s = 8.6 \times 10^{-4}$ Ω and $\eta = 3.4$ are obtained as fitting parameters for DHL1, and $R_s = 7.5 \times 10^{-6}$ Ω and $\eta = 4.4$ are obtained for DHL2.

2.6. Discussion on the Microscopic Mechanism

The microscopic mechanism of the trapping of Cooper pairs in the DNRs remains elusive, and the DHLs provide critical reference for our discussion on the following two possible mechanisms:

1) In 1D superconducting nanowires, a minute resistance peak was occasionally found to be superimposed on the pronounced superconducting gap in $R(H)$.[41] Such observations are commonly attributed to phase slips caused by the tunneling of flux quanta across the nanowires. The constituent nanowires of our DNRs and DHLs are, however, located in the 3D regime. If the giant negative "magnetoresistance" were caused by phase slips taking place at the grain boundaries (weak links), the DHLs would have shown a similar "magnetoresistance" with an amplitude comparable to that of the DNRs, which clearly contradicts our experimental data (Figure 4). Moreover, as the fingerprint of phase slips, the $V(I)$ dependences of 1D superconducting nanowires generally show a number of resistive steps below T_c, whereas no such resistive steps are observed in the DNRs and DHLs (Figure 5).

2) Electrons can form standing waves when being forced to remain within a limited region in space. An intriguing question is whether Cooper pairs can form bosonic standing waves. Assuming that bosonic standing waves are formed through the interference between the superconducting waves traveling in *opposite* directions (clockwise and counterclockwise) along the two branches of a DNR, the Cooper pairs will be trapped in a quantum-well-like DNR (Figure 7c), thus giving rise to the anomalous metal–bosonic semiconductor transition.

**ADVANCED
SCIENCE NEWS**

www.advancedsciencenews.com

**ADVANCED
MATERIALS**

www.advmat.de

In the presence of different grain boundaries and structural imperfections in their constituent diamond nanowires, the phase difference between the opposite propagating bosonic waves in DNR1 and DNR2 can be different, and a more destructive interference in DNR2 can be responsible for its lower amplitude of the resistance anomaly in $R(T)$ and $R(H)$.

In contrast, the Cooper pairs in a DHL can only flow in the same direction, thus making a superconducting transition feasible. This assumption can also explain the absence of Little–Parks oscillations in the DNRs (Figures 2 and 6).[42] When applying magnetic fields in the axial direction of a superconducting loop, as in our measurements on the DNRs, the phase of the superconducting wavefunction may increase by an integer multiple of 2π with every rotation around the loop axis. In this case, the magnetic flux, $\Phi = \int_L A \cdot \mathrm{d}l$, threading the loop, L,[43] is quantized in multiples of the flux quantum, $\Phi_0 = h/2e$, where A is the magnetic vector potential, dl is the loop boundary, h is the Planck constant, and $2e$ is the charge of a Cooper pair. Due to the flux quantization, T_c and the resistance in the vicinity of T_c are both periodic functions of Φ enclosed in the loop, known as the Little–Parks effect. If there are Cooper pairs circulating in opposite directions (clockwise and counterclockwise) in a DNR, the path integrals along dl and −dl will cancel each other out, leading to $\Phi = 0$ and thus the absence of Little–Parks oscillations.

Another possible cause of the absence of Little–Parks oscillations in the DNRs can be related to the grain boundaries in the constituent nanowires. In the presence of the weak links at the grain boundaries, the phase differences between neighboring grains will add to the phase increase of the superconducting wavefunction with every rotation around L. In this case, the resulting phase increase with every rotation around L is unnecessarily equal to $2\pi n$ (n is an integer), and thus Φ can be unequal to $n\Phi_0$. In the absence of flux quantization, the Little–Parks effect will not take place in the DNRs.

3. Conclusion

We demonstrated that other than transforming into a superconductor or a quantum metal, an established metallic material can instead approach zero temperature by converting into a bosonic semiconductor. We interpreted the emergence of the bosonic semiconducting phase in the DNRs as being a result of the formation of trapped Cooper pairs at the expense of free electrons. Our data add to the existing categories of magnetoresistance, that is, the giant magnetoresistance in magnetic multilayers,[35] the colossal magnetoresistance in perovskite manganites,[44] and the geometric magnetoresistance in semiconductor–metal hybrids,[45] by providing an unconventional giant negative "magnetoresistance" with bosonic nature. In contrast to the conventional giant magnetoresistance caused by spin-dependent scattering, the unconventional giant "magnetoresistance" in the bosonic semiconducting DNRs arises from the breaking of trapped Cooper pairs by applied magnetic fields. Our findings call for follow-up investigations of the influence of different variables on the unconventional giant "magnetoresist-

ance" in DNRs. Our results imply that apart from being engineered into superconducting quantum interference devices for magnetometry, DNRs could be used as cavities to trap Cooper pairs for potential applications in other quantum devices, for example, artificial atoms for qubits.

4. Experimental Section

Diamond Growth: The DTFs were grown using hot filament CVD. Prior to CVD, undoped Si (100) substrates with a 300 nm-thick layer of SiO_2 were cleaned in acetone and then isopropanol for 15 min each and subsequently rinsed with deionized water in an ultrasonic bath. The substrates were then seeded with nanodiamond particles with an average particle size of 3.3 ± 0.6 nm (NanoCarbon Research Institute Ltd., Japan) using an electrospray deposition technique.[28] The CVD process used a gas mixture containing 1% CH_4 in H_2 together with B_2H_6 (at a B:C ratio of 8750 ppm) controlled using independent mass flow controllers. The hot tantalum filament (>2000 °C) thermally decomposed the gases into reactive atoms and radicals at 20 Torr, causing the deposition of a continuous boron-doped diamond layer. The deposition was for 1 h resulting in polycrystalline DTFs of thickness ≈500 nm. The boron concentration of the DTFs was determined to be about 3.3×10^{21} cm^{-3} through Hall effect measurements previously calibrated with secondary ion mass spectrometry (SIMS). The mean grain size of the DTFs was obtained by analyzing scanning electron microscopy (SEM) images with ImageJ software.

Fabrication of Diamond Microcrosses: An electron-beam lithography facility (ELS-7500EX) with an acceleration voltage of 50 kV and an electron-beam current of ≈1 nA was first used to define microcrosses on the DTFs. After developing the photoresist, a 100nm-thick Al layer was deposited onto the patterned DTFs by electron-beam evaporation (base pressure of about 10^{-5} Pa) to act as a mask for reactive ion etching (RIE). The RIE process was performed in a 13.56 MHz inductively coupled plasma reactor (ULVAC CE300I) in an oxygen atmosphere with a flow rate of 90 sccm at 0.5 Pa. The chamber power was 800 W, which was combined with a bias power of 20 W applied to the substrate electrode to facilitate anisotropic etching. The RIE process was automatically stopped once the Si substrate was reached, as confirmed by a profilometer measuring the etching depth. Afterward, the Al mask was chemically removed in a solution of trimethylamine. After ultrasonically cleaning the samples in deionized water, a laser lithography process was adopted to define the electrode areas. A bilayer of Ti (10 nm)/Au (100 nm) was deposited as the contact pads by using electron-beam evaporation, as before. After the lift-off process, the samples were ultrasonically cleaned in acetone, methanol, and then deionized water.

Focused Ion Beam Milling: Following the microfabrication, an FEI Helios FIB/SEM DualBeam was used to pattern the diamond microcrosses into DNRs and DHLs. The Ga ion source was operated at an acceleration voltage of 30 kV. The patterning was performed using a two-step method: 1) rough patterning with a beam current of 0.43 nA for the preparation of trenches; 2) fine cleaning by using a beam current of 0.23 nA–80 pA to suppress the beam damage to the diamond nanowires and to ensure the correct linewidth. During the ion milling, despite vacuum pumping, a thin layer of high-resistance amorphous carbon was redeposited onto the surface of the DNRs and DHLs, which smears out the height difference between the diamond crystallites and enshrouds the grain boundaries (a few atomic layers thick), making the grain boundaries invisible on SEM images (Figures 2 and 4).

Electrical Transport Measurements: The electrical transport properties of the samples were characterized through four-probe measurements in a ^{3}He/^{4}He closed-cycle dry cryostat equipped with a d.c. magnet (ICE Oxford). A low-frequency excitation current of 5 µA and a lock-in amplifier were used to measure the temperature and magnetic-field dependences of resistance. Magnetic fields were applied in the out-of-plane direction for all measurements. The $V(I)$ measurements were performed by sending d.c. currents through the devices.

Conflict of Interest

The authors declare no conflict of interest.

Data Availability Statement

The data that support the findings of this study are available from the corresponding author upon reasonable request.

[1] J. G. Bednorz, K. A. Müller, *Z. Phys. B: Condens. Matter* **1986**, *64*, 189.

[2] E. Morosan, D. Natelson, A. H. Nevidonskyy, Q. Si, *Adv. Mater.* **2012**, *24*, 4896.

[3] Y. Kamihara, H. Hiramatsu, M. Hirano, R. Kawamura, H. Yanagi, T. Kamiya, H. Hosono, *J. Am. Chem. Soc.* **2006**, *128*, 10012.

[4] Z.-A. Ren, Z.-X. Zhao, *Adv. Mater.* **2009**, *21*, 4584.

[5] M. Osada, B. Y. Wang, B. H. Goodge, S. P. Harvey, K. Lee, D. Li, L. F. Kourkoutis, H. Y. Hwang, *Adv. Mater.* **2021**, *33*, 2104083.

[6] T. Soma, K. Yoshimatsu, A. Ohtomo, *Sci. Adv.* **2020**, *6*, eabb8570.

[7] S. Zeng, C. Li, L. E. Chow, Y. Cao, Z. Zhang, C. S. Tang, X. Yin, Z. S. Lim, J. Hu, P. Yang, A. Ariando, *Sci. Adv.* **2022**, *8*, eabl9927.

[8] E. A. Ekimov, V. A. Sidorov, E. D. Bauer, N. N. Mel'nik, N. J. Curro, J. D. Thompson, S. M. Stishov, *Nature* **2004**, *428*, 542.

[9] G. Zhang, S. Turner, E. A. Ekimov, J. Vanacken, M. Timmermans, T. Samuely, V. A. Sidorov, S. M. Stishov, Y. Lu, B. Deloof, B. Goderis, G. Van Tendeloo, J. Van De Vondel, V. V. Moshchalkov, *Adv. Mater.* **2014**, *26*, 2034.

[10] C. An, Y. Zhou, C. Chen, F. Fei, F. Song, C. Park, J. Zhou, H.-G. Rubahn, V. V. Moshchalkov, X. Chen, G. Zhang, Z. Yang, *Adv. Mater.* **2020**, *32*, 2002352.

[11] J. Guo, G. Lin, S. Cai, C. Xi, C. Zhang, W. Sun, Q. Wang, K. Yang, A. Li, Q. Wu, Y. Zhang, T. Xiang, R. J. Cava, L. Sun, *Adv. Mater.* **2019**, *31*, 1807240.

[12] R. Nigam, A. V. Pan, S. X. Dou, *Phys. Rev. B* **2008**, *77*, 134509.

[13] P. Santhanam, C. C. Chi, S. J. Wind, M. J. Brady, J. J. Bucchignano, *Phys. Rev. Lett.* **1991**, *66*, 2254.

[14] V. V. Moshchalkov, L. Gielen, G. Neuttiens, C. Van Haesendonck, Y. Bruynseraede, *Phys. Rev. B* **1994**, *49*, 15412.

[15] M. Park, M. S. Isaacson, J. M. Parpia, *Phys. Rev. B* **1997**, *55*, 9067.

[16] H. Wang, M. M. Rosario, H. L. Russell, Y. Liu, *Phys. Rev. B* **2007**, *75*, 064509.

[17] A. Harada, K. Enomoto, T. Yakabe, M. Kimata, H. Satsukawa, K. Hazama, K. Kodama, T. Terashima, S. Uji, *Phys. Rev. B* **2010**, *81*, 174501.

[18] M. A. Crusellas, J. Fontcuberta, S. Piñol, *Phys. Rev. B* **1992**, *46*, 14089.

[19] M. Suzuki, *Phys. Rev. B* **1994**, *50*, 6360.

[20] C. Buzea, T. Tachiki, K. Nakajima, T. Yamashita, *IEEE Trans. Appl. Supercond.* **2001**, *11*, 3655.

[21] Y. M. Wan, S. E. Hebboul, D. C. Harris, J. C. Garland, *Phys. Rev. Lett.* **1993**, *71*, 157.

[22] E. Silva, M. Lanucara, R. Marcon, *Phys. C* **1997**, *276*, 84.

[23] P. Lindqvist, A. Nordström, Ö. Rapp, *Phys. Rev. Lett.* **1990**, *64*, 2941.

[24] T. G. Berlincourt, *Phys. Rev.* **1959**, *114*, 969.

[25] P. Achatz, W. Gajewski, E. Bustarret, C. Marcenat, R. Piquerel, C. Chapelier, T. Dubouchet, O. A. Williams, K. Haenen, J. A. Garrido, M. Stutzmann, *Phys. Rev. B* **2009**, *79*, 201203(R).

[26] G. Zhang, M. Zeleznik, J. Vanacken, P. W. May, V. V. Moshchalkov, *Phys. Rev. Lett.* **2013**, *110*, 077001.

[27] M. V. Feigel'man, A. I. Larkin, M. A. Skvortsov, *Phys. Rev. Lett.* **2001**, *86*, 1869.

[28] P. W. May, *Philos. Trans. R. Soc. London, Ser. A* **2000**, *358*, 473.

[29] G. Zhang, T. Samuely, F. Du, Z. Xu, L. Liu, O. Onufriienko, P. W. May, J. Vanacken, P. Szabó, J. Kačmarčík, H. Yuan, P. Samuely, R. E. Dunin-Borkowski, J. Hofkens, V. V. Moshchalkov, *ACS Nano* **2017**, *11*, 11746.

[30] P. W. May, W. J. Ludlow, M. Hannaway, P. J. Heard, J. A. Smith, K. N. Rosser, *Diamond Relat. Mater.* **2008**, *17*, 105.

[31] J. F. Ziegler, J. P. Biersack, U. Littmark, *The Stopping and Range of Ions in Solids*, Pergamon Press, New York **1984**.

[32] E. Bustarret, J. Kačmarčík, C. Marcenat, E. Gheeraert, C. Cytermann, J. Marcus, T. Klein, *Phys. Rev. Lett.* **2004**, *93*, 237005.

[33] P. Schofield, A. Bradicich, R. M. Gurrola, Y. Zhang, T. D. Brown, M. Pharr, P. J. Shamberger, S. Banerjee, *Adv. Mater.* **2022**, https://doi.org/10.1002/adma.202205294.

[34] T. I. Baturina, A. Y. Mironov, V. M. Vinokur, M. R. Baklanov, C. Strunk, *Phys. Rev. Lett.* **2007**, *99*, 257003.

[35] M. N. Baibich, J. M. Broto, A. Fert, F. Nguyen Van Dau, F. Petroff, P. Etienne, G. Creuzet, A. Friederich, J. Chazelas, *Phys. Rev. Lett.* **1988**, *61*, 2472.

[36] M. Tinkham, *Introduction to Superconductivity*, McGraw-Hill, New York **2004**.

[37] B. Sacépé, T. Dubouchet, C. Chapelier, M. Sanquer, M. Ovadia, D. Shahar, M. Feigel'Man, L. Ioffe, *Nat. Phys.* **2011**, *7*, 239.

[38] C. Renner, B. Revaz, J.-Y. Genoud, K. Kadowaki, Ø. Fischer, *Phys. Rev. Lett.* **1998**, *80*, 149.

[39] S. Li, H. Yang, D. Fang, Z. Wang, J. Tao, X. Ding, H. Wen, *Sci. China: Phys., Mech. Astron.* **2013**, *56*, 2019.

[40] M. Kugler, Ø. Fischer, C. Renner, S. Ono, Y. Ando, *Phys. Rev. Lett.* **2001**, *86*, 4911.

[41] X. D. A. Baumans, D. Cerbu, O.-A. Adami, V. S. Zharinov, N. Verellen, G. Papari, J. E. Scheerder, G. Zhang, V. V. Moshchalkov, A. V. Silhanek, J. Van de Vondel, *Nat. Commun.* **2016**, *7*, 10560.

[42] W. A. Little, R. D. Parks, *Phys. Rev. Lett.* **1962**, *9*, 9.

[43] F. London, *Phys. Rev.* **1948**, *74*, 562.

[44] M. Uehara, S. Mori, C. H. Chen, S.-W. Cheong, *Nature* **1999**, *399*, 560.

[45] S. A. Solin, T. Thio, D. R. Hines, J. J. Heremans, *Science* **2000**, *289*, 1530.